Insulin Hexamer Dissociation Dynamics Revealed by Photoinduced T-jumps and Time-Resolved X-Ray Solution Scattering

Journal:	*Photochemical & Photobiological Sciences*
Manuscript ID	PP-COM-01-2018-000034.R1
Article Type:	Communication
Date Submitted by the Author:	13-Apr-2018
Complete List of Authors:	Rimmerman, Dolev; Northwestern University Department of Chemistry, chemistry Leshchev, Denis; Northwestern University, Chemistry Hsu, Darren; Northwestern University, Chemistry Hong, Jiyun; Northwestern University, Chemistry Abraham, Baxter; University of Delaware, Department of Chemistry and Biochemistry Henning, Robert; University of Chicago, CARS Kosheleva, Irina; The University of Chicago Chen, Lin; Northwestern University, Chemistry; Argonne National Laboratory, Chemical Sciences and Engineering

Photochemical & Photobiological Sciences

COMMUNICATION

Insulin Hexamer Dissociation Dynamics Revealed by Photoinduced T-jumps and Time-Resolved X-Ray Solution Scattering

Received 00th January 20xx,
Accepted 00th January 20xx

DOI: 10.1039/x0xx00000x

www.rsc.org/

Dolev Rimmerman,[a] Denis Leshchev, [a] Darren J. Hsu, [a] Jiyun Hong, [a] Baxter Abraham, [b] Irina Kosheleva, [c] Robert Henning, [c] Lin X. Chen*[a,d]

The structural dynamics of Insulin hexamer dissociation were studied by photoinduced temperature jump technique and monitored by time-resolved x-ray scattering. The process of hexamer dissociation was found to involve several transient intermediates, including an expanded hexamer and an unstable tetramer. Our findings provide insights into the mechanisms of protien-protein association.

Protein-protein interactions often lead to the assembly of quaternary structures, which are utilized *in-vivo* to regulate function or as a means of storage.[1,2] However, some protein interactions may also have undesirable outcomes, such as protein aggregation, which can result in the formations of fibrils that are associated with neurodegenerative deseases.[3,4] Insulin is a 51-amino acid endocrine hormone that plays an important role in the regulation of blood-glucose levels.[5] *In-vivo*, insulin monomers assemble into hexamers so that they can be stored in an inactive state until they are ready to be released into the bloodstream.[6,7] Upon release, the insulin hexamers dissociate into monomers that can bind to the insulin receptor.[8,9] However, insulin subunits also have a tendency to aggregate to form fibrils, an undesirable process that primarily occurs from the monomer, rather than the hexamer state.[6] Therefore, an understanding of insulin oligomerization dynamics can provide insights into the protein-protein interactions that govern protein association mechanisms, which result in native function, as well as disease.

Insulin has been extensively studied as a model system for protein oligomer and fibril formation due to its ability to form a variety of native associative states, primarily monomers, dimers and hexamers.[8–14] The insulin association mechanism is dependent on the starting assembling states (e.g., monomers, dimers, etc.). Insulin dimers associate through the formation of an intermolecular beta sheet that connects two monomers together.[14] In contrast, hexamers form by association through an interface between dimers, typically in the presence of zinc ions.[9] As a result, the formation of different assembling states is expected to progress through different pathways and characteristic dynamics. The insulin assembling state is known to be tuneable by environmental conditions, such as solvent composition, temperature and pH. Specifically, in the presence of EtOH and low pH, the assembling state of the protein becomes temperature dependant in the range of 10-50 °C, with monomers comprising the primary species at 50 °C, dimers as the primary species at 30 °C and higher order oligomers at 15 °C and lower.[11,14,15]

Protein association dynamics typically follow a diffusion limited process, in which the constituents must form an encounter complex, and thus processes that are faster than diffusion are typically obscured in ensemble kinetic experiments. One way to overcome this barrier is to study these later steps in association dynamics by investigating the reverse, first-order process of dissociation.[14,15] For temperature sensitive oligomer systems, such as insulin, a laser-induced temperature jump (T-Jump) can be used to perturb the chemical equilibrium between the constituent units and the oligomer to create a non-equilibrium state in which the oligomer state is overpopulated, and therefore driving the reaction towards the formation of constituent units.[16] Laser induced experiments allow for the ensemble to be effectively synchronized to a higher temperature state within nanoseconds, therefore allowing the temporal resolution needed for the detection of short-lived early intermediates in the dissociation process.[14,15,17] These early steps of dissociation mirror the late stages of association in reverse order, and therefore allow these processes to be studied by circumventing the process of diffusion. In the case of insulin, T-jump experiments have been demonstrated to

[a] *Department of Chemistry, Northwestern University, Evanston, Illinois 60208, USA E-mail: l-chen@northwestern.edu*
[b] *Department of Chemistry and Biochemistry, University of Delaware, Newark, Delaware 19716, USA*
[c] *Center for Advanced Radiation Sources, The University of Chicago, Illinois 60637, USA*
[d] *Chemical Sciences and Engineering Division, Argonne National Laboratory, Argonne, Illinois 60439, USA E-mail: lchen@anl.gov*

Electronic Supplementary Information (ESI) available. See DOI: 10.1039/x0xx00000x

successfully initiate a dimer dissociation reaction, which was then tracked by time-resolved techniques, including 2D-IR spectroscopy and time-resolved x-ray solution scattering (TRXSS).[14,15] These works revealed, through the study of the early steps of dimer dissociation, that the late steps of dimer formation are strongly coupled to solvent degrees of freedom and include multiple restructuring steps prior to achieving the final dimer state.

Here we advance on the previous studies by investigating the structural dynamics of insulin hexamer dissociation to gain insights into short lived intermediates in the late stages of insulin hexamer formation. Hexamer dissociation dynamics were initiated by applying a nanosecond T-jump from a low temperature state (15 °C) and directly observed the resulting conformational dynamics with TRXSS. X-ray solution scattering is a common technique for revealing protein structure for samples that cannot be crystallized or where the solution structure varies significantly from the crystal structure.[18–20] The technique is sensitive to protein secondary and tertiary structures, as well as changes in density and mass.[21–29] For this reason, TRXSS experiments are especially suitable for investigating protein structural dynamics, and, in particular, protein folding and association.[15,19,22,24–27,29,30] Moreover, TRXSS is suitable for probing proteins in undeuterated (native) water environment and does not require the use of fluorescent labelling, therefore it provides direct structural information that complements with inferred structural information obtained by other optical methods, such as optical absorption, UV-circular dichroism (UV-CD), and IR spectroscopy. Finally, TRXSS signals are not only sensitive to protein structure, but also to bulk solvent structural changes caused by thermal effects, thus providing an inherent temperature probe directly within the T-jump experiment.[15,21,31] Coupled to T-jumps, TRXSS therefore represents a suitable tool for monitoring complex protein dynamics with high structural sensitivity and high temporal resolution.

Results and discussion

The assembling states of bovine insulin in an aqueous mixture of 20% v/v ethanol at low pH (0.27M HCl) were examined by UV-CD and small angle x-ray scattering (SAXS) at different temperatures in the range of 15-50 °C. The details of these experiments and sample preparation have been described previously.[15] We have also previously reported the characteristics of insulin dimers and monomers using UV-CD and SAXS in the temperature range of 25-50 °C, and the latter method suggested a radius of gyration (R_g) increase from ~13 Å for monomers to ~15 Å for dimers.[15] Complementing the previous results, we observe in the current study that when the system is cooled down from 25 to 15 °C the average R_g changes rapidly from ~15 Å to ~18 Å, an increase that deviates from the trend observed between 25 – 50 °C, indicating the formation of oligomers larger than the dimers. A summary of

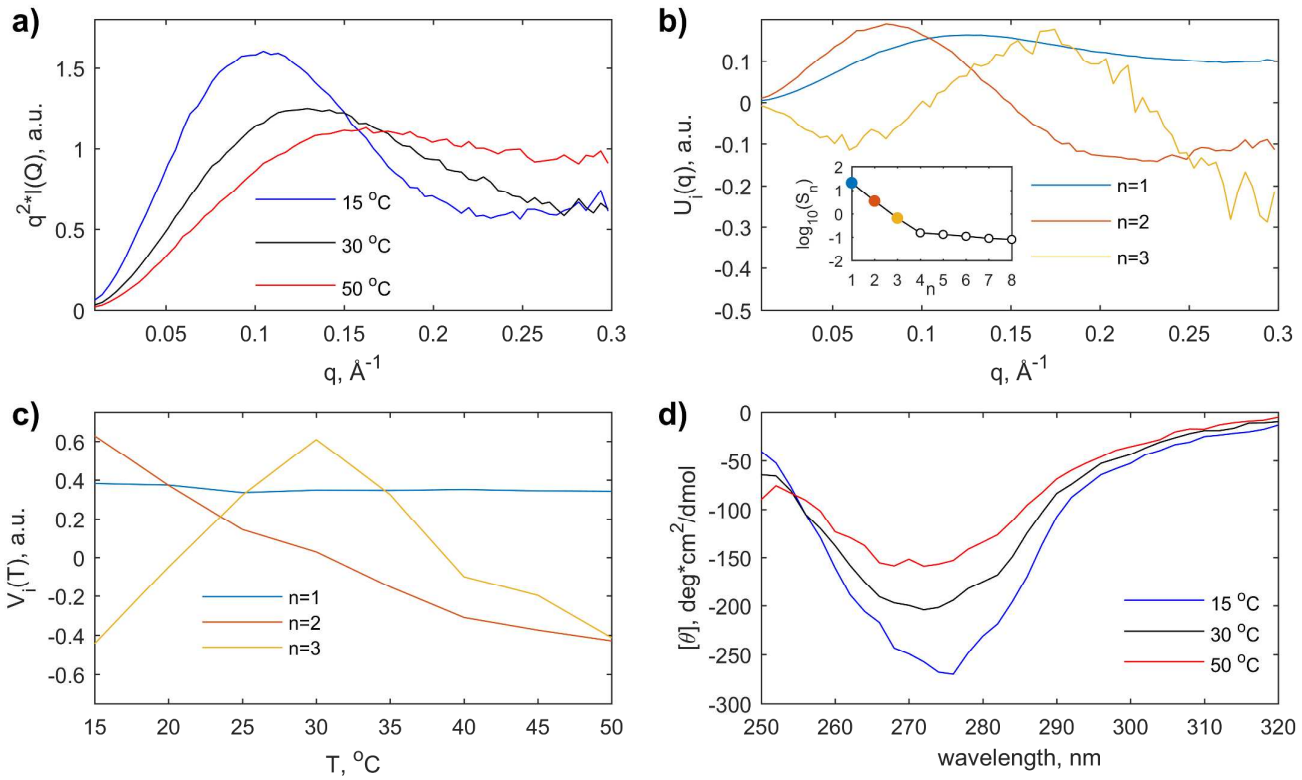

Figure 1. (a) Representative Kratky curves for bovine insulin under low pH conditions in aqueous-EtOH solution at 15, 30 and 50 °C representing the three major species . (b) SVD decomposition results from Kratky plot analysis, the main figure shows the left -singular vectors and the inset shows the associated singular values. (c) SVD decomposition results from Kratky plot analysis, the figure shows the right-singular vectors (d) UV-CD spectra for tyrosyl absorption band at different temperatures.

the SAXS data in Kratky plot form from the previous study (30 and 50 °C) and current study (15 °C), are shown in Figure 1. The Kratky representation plots scattering intensity multiplied by q^2 as a function of q, the transferred momentum. Since scattering intensity of globular proteins is typically proportional to q^{-4} in the Porod region of the scattering curve, such proteins will present a bell shaped curve in the Kratky representation.[32] However, unfolded and flexible proteins will deviate from the expected behaviour in the Porod region and would therefore lose their expected bell-shape. The bell-shape of Kratky curves at 0.1 - 0.2 $Å^{-1}$ shows that the insulin conformation remains folded at all examined temperatures and agree with the Kratky plots for insulin that were previously reported by Ahmad et al.[8]. However, the bell shape of the Kratky curves becomes significantly narrower at lower temperatures (below 25 °C) and adopts a tighter Gaussian shape even at high q values (q > 0.1 $Å^{-1}$) that is significantly different in shape than the curves at higher temperatures. In addition, the maximum intensity of the Kratky plot shifts to smaller q values at lower temperature, indicating an increase in the assembled protein size, confirming the formation of a larger oligomer state as temperature decreases. The changes in the Kratky curve at lower temperatures suggests that, on average, the corresponding species are significantly larger and more rigid than the dimers or monomers present at higher temperatures, In order to verify that only three insulin assembling states (i.e. monomers, dimers and oligomers) are present in the entire temperature range of the experiment (i.e., 15 – 50 °C), Kratky plots were analysed by singular value decomposition (SVD) based on eight curves (15 – 50 °C with 5 °C increments). SVD is a standard tool for analysis of both static and time-resolved scattering datasets.[26,33–35] This mathematical decomposition procedure provides information about the number of distinct species whose linear combination comprise the entire dataset. The large amplitudes of the first three singular values along with pronounced shapes of left and right singular vectors clearly demonstrate that only three species exist across the entire temperature range (see Figure 1b, c), confirming the premise that only one type of oligomers forms below 25 °C. In contrast, our previously reported SVD analysis of the Kratky curves from the temperature range of 25 – 50 °C showed presence of only two significant SVD components that reflects the prevalence of monomers and dimers at these temperatures.[15]

The insulin dimers can serve as building blocks for several larger oligomers, for example, tetramers, hexamers or fibrils. Uversky et al. reported on the spectroscopic characteristics of insulin oligomers originating from mutant variants and found that the UV-CD signal for the tyrosyl absorption band (275 nm) remained relatively constant between dimers and tetramers, however it became significantly more negative for the hexamer state relative to either dimer or tetramer.[8,9] Our UV-CD results, shown in figure 1d, indicate that the molar ellipticity of tyrosyl absorption becomes substantially more negative as temperature decreases. Taken together with the trend in R_g from SAXS measurements, the UV-CD results therefore indicate that at lower temperature the association state is driven towards the formation of hexamers rather than tetramers. Furthermore, previous works have established that in native insulin, the majority species include only hexamers, dimers and monomers.[36,37] The appearance of other, high order oligomers, such as fibrils is unlikely, as this would cause a dramatic increase in forward scattering and very large R_g changes, as well as changes in form factor and they are likely to disassemble with temperature. For this reason, we surmise that at 15 °C insulin exists as a mixture of hexamers and dimers as the primary species. It is also apparent that the 15 °C state does not represent a complete transformation of the dimers into hexamers, but instead is a mixture of hexamers with a large population of dimers. Therefore, the R_g and UV-CD values represent an average based on the mixture of populations. However, when lowering the temperature below 15 °C to increase the population of hexamers, we observed precipitation of the insulin, which is expected due to the poor solubility of the hexamer form.[7,38] Therefore 15 °C represents the lowest temperature that could be reliably measured in the experiment.

As we are clear about the temperature dependence of the insulin assembling states, we now can study the dynamics of their transformation by perturbing the equilibrium with T-jump. The T-jump TRXSS experiments were carried out at Beamline 14ID, the BioCARS, in the Advanced Photon Source (APS) at Argonne National Laboratory.[39] The details of T-jump TRXSS experiments and sample preparation have been described previously.[15] In brief, ns-laser pulses set at 1443 nm wavelength were used to excite an overtone of O-H vibration in the solvent to generate an ~8 °C temperature jump. TRXSS was used to probe the resulting protein structural dynamics from the nano- to millisecond timescales. X-ray scattering patterns, measured by a 2D camera, were azimuthally integrated and used to calculate one-dimensional scattering difference curves ΔS(q,t) (with q and t being transferred momentum and time delay, respectively) according to standard procedures.[15,39] The sample was loaded into a temperature controlled capillary flow cell by syringe pump and the sample volume was discarded after each laser/x-ray interaction in order to prevent accumulation of x-ray damage. Short time delay data (< 5 μs) was taken utilizing a single x-ray pulse (FWHM ~100 ps) extracted from the x-ray pulse train running at a 6.5-MHz repetition rate. For longer time delays (> 10 μs), TRXSS data was taken utilizing 24 bunches chopped from the synchrotron source (~3.6 μs time resolution). The initial experimental temperature of 15°C was chosen because the scattering signal from protein build-up on the capillary wall appears due to a lower insulin solubility at temperature ≤ 10 °C.

The results of the TRXSS experiments are summarized in figure 2. TRXSS differential signals typically contain contribution from both protein and solvent density changes. In order to derive the protein-associated portion of the signal we conducted a pure-solvent TRXSS measurement, which was then fitted to the signal in the wide angle (WAXS) region at q > 0.5 $Å^{-1}$. The WAXS signal in this region contains mainly contribution from water and EtOH mixture, therefore it was

used to obtain the changes in the temperature of the system as a function of time. The fitted solvent contributions were subtracted from the TRXSS curve recorded on insulin solution.

SVD analysis was performed in order to extract the number of the transient species captured in this experiment (see Supporting Information for details). The analysis shows the

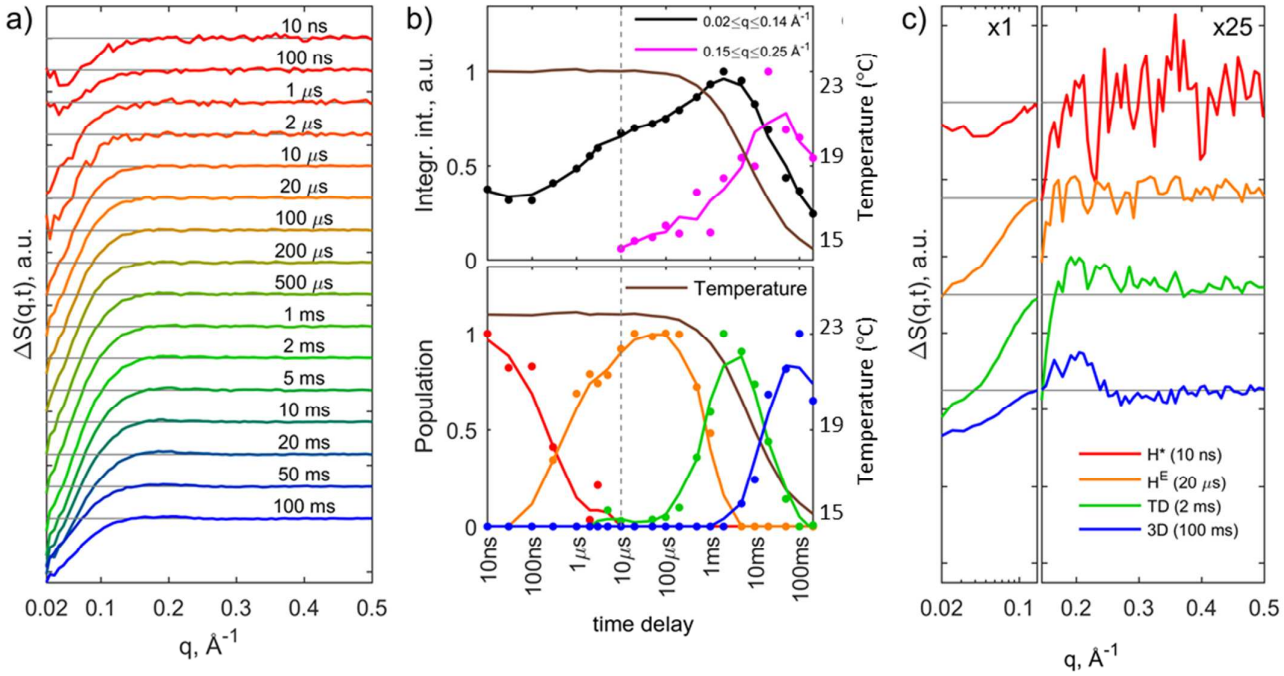

Figure 2. (a) Protein associated TRXSS data for representative time delays. (b) (top) Progression of normalized integrated intensity of protein associated TRXSS signals in two regions shown along with the dynamics of normalized temperature jump. The dashed line separates the data collected for time delays <10 μs and data collected for time delays >10 μs, which have different signal-to-noise ratio as explained in the main text. The integrated values for 0.15≤q≤0.25 Å^{-1} region at <10 μs are omitted due to low signal-to-noise ratio. The lines represent a guide for the eye calculated using Savitzky-Golay linear three point filter on the data points. (b) (bottom) Magnitude of components derived from linear combination analysis by utilizing four representative differential scattering curves. The lines represent a guide for the eye calculated similarly to the b, top panel. (c) Selected TRXSS curves for linear combination analysis representing signals corresponding to the species predominantly present in the solution at corresponding time delays. For q>=0.145 Å^{-1} the data is multiplied by 25 for clarity.

The time series of protein associated TRXSS signals (after solvent subtraction) is presented in Figure 2a. It is clear that the protein structural signal appears in the SAXS region (q < 0.15 Å^{-1}) even at the shortest time delay (i.e. 10 ns, the laser pulse duration is 7 ns). In order to quantify the progression of this signal, the SAXS region was integrated and plotted as a function of time delay along with the evolution of the system temperature (Figure 2b, top). The integration reveals that at least two processes occur following excitation. First, a signal arises at the shortest time delay (10 ns) and remains relatively constant until 100 ns, when an intensity of the SAXS signal grows rapidly on the microsecond timescale. After short flattening around 10 μs, the SAXS signal further grows until 2 ms which is followed by a decay at longer timescales as the system cools back down to equilibrium. In addition, we observe a formation of positive feature in the WAXS region, around q ~ 0.2 Å^{-1}, after 10 μs. Following the evolution of this feature by integrating its intensity, we observe that the WAXS feature grows concurrently with the SAXS signal up until 2 ms. However, while the SAXS intensity starts to decay at later time delays, the WAXS feature keeps growing until ~20 ms and only then starts to decay.

existence of four states, two of which are observed prior to the system cool-down and the other two are observed during system cool-down. These observations coincide with noticeable changes in the scattering patterns at different time delays as revealed by the inspection of integrated signals, as well as scattering difference patterns. To retrieve the characteristic timescales associated with the transitions between the intermediate species, we performed a simple exponential fitting of the data by using the SVD results (see SI). We found that four exponential terms were sufficient for reproducing the data and the following characteristic time scales were retrieved from the fitting: 0.9 ± 0.1 μs, 730 ± 20 μs, 20.5 ± 0.7 ms and 300 ± 15 ms. Since two of these timescales coincide with the system cool-down, which ensues in the time range between 1 ms and 1 s (Figure 2b), finding an adequate kinetic model to describe the system evolution is non-trivial. For this reason, we chose to model the systems using linear combination analysis (LCA).

LCA is a common method for reproducing time delay data in TRXSS experiments by utilizing representative scattering difference patterns from major emergent species.[26] LCA does not produce pure species associated scattering curves due to the reliance of the method on representative time delay

curves. However, as opposed to other analysis methods, such as global analysis, LCA does not require assumption about kinetic models that may be affected by temperature changes and therefore is more suitable for these TRXSS experimental results. Based on the integration results and the obtained timescales, we have chosen four time delays as the basis for the LCA, namely, 10 ns, 20 μs, 2 ms and 100 ms. These time delays represent time points at which the TRXSS integral signal plateaus, indicating the saturation of the transition between states and that the signal is dominated by one of the species. Fitting the data with selected curves gives a satisfactory agreement and allows us to obtain the time dependent contribution of each of the species. The population of each of the species and the corresponding curves, used for fitting the data, are shown in Figure 2b and 2c.

The first species appears at earliest time point probed in the experiment (10 ns) and its signal remains mostly unchanged until 100 ns. The scattering difference signal shows a noticeable loss of scattering in the SAXS region without additional features (Figure 2c), indicating that the protein volume undergoes expansion. Given that quick appearance of the state (<10 ns), we associate this early intermediate (H^*) with a hot protein state due to the laser induced heating of the solvent, which is expected to cause slight expansion of the protein due to the thermal-induced loss of hydrogen bonding that leads to loss of protein density and increased solvent exposure.

The second state H^E (expanded hexamer) rises on 0.9 ± 0.1 μs timescale with a large decrease in forward scattering that comprises the bulk of the difference signal. By inspecting the representative TRXSS signal recorded at 20 μs, we observe further loss of scattering intensity in the SAXS region ($q < 0.15 Å^{-1}$) compared to 10 ns, which indicates further reorganization of the protein structure due to heating. The further loss of forward scattering relative to the H^* state indicates that the protein restructures to become significantly more expanded. However, the lack of WAXS features (at $q > 0.15$ $Å^{-1}$), which are expected to arise when the hexamer dissociates to dimer, as apparent from the reference difference calculated using static SAXS data recorded at 15 and 20 °C (see reference static difference curve in figure 3), indicate that the protein retains its hexamer form. The presence of the H^E state suggests that prior to dissociation into dimers, the hexamer evolves to an intermediate state in which it assumes a partially unfolded and flexible conformation, as evidenced by the expansion observed in the SAXS region of the signal. Finally, based on the integration results, it is apparent that the formation of the H^E state involves a significant rise in integrated SAXS intensity from ~30 % to 70% of the maximum integral value, indicating that the formation of this state encompasses most of the hexamer structural rearrangement prior to dissociation.

The final two states arise on significantly longer timescales, specifically the TD (tetramer + dimer) state with 730 ± 20 μs lifetime and the 3D (three dimer) state with 20.5 ± 0.7 ms lifetime. The difference scattering signals of both states show loss of intensity in the SAXS region, as well as

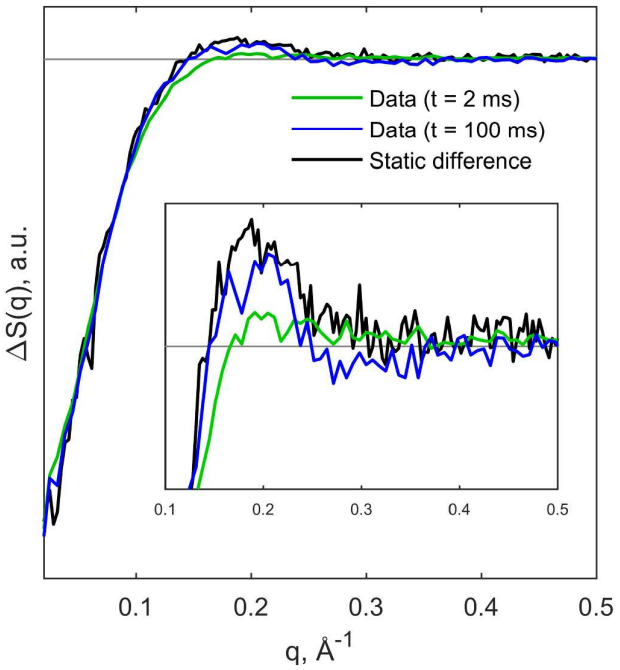

Figure 3. Comparison of the protein associated TRXSS data recorded at 2ms and 100 ms time delays with reference difference data calculated from static SAXS curves collected at 20 and 15 °C.

appearance of WAXS features, most prominently a positive peak at $0.15 < q < 0.3$ $Å^{-1}$ (see figure 3). Moreover, as the TD state evolves into the 3D state, the WAXS peak shifts to smaller angles, indicating structural differences between the two states. To assess the nature of these states, we compared both difference patterns to the reference difference calculated using static SAXS data recorded at 15 and 20 °C that corresponds to transition from hexamers to dimers (Figure 3). The reference curve fits the 3D difference significantly better than the TD difference, especially in the WAXS region, indicating that the species predominant at later time delays corresponds to dimers at the final stage of hexamer dissociation. In addition, we have found a qualitative agreement between the TRXSS data recorded at 100 ms and the theoretical curve calculated by taking a difference between crystal structures of hexamer and dimers, which further supports the structural assignment of the 3D state (see SI for details).

The penultimate TD state exhibits a WAXS feature that is similar to the 3D state, but with much smaller intensity (see inset in figure 3), which likely indicates a partially dissociated state. We assign this partially dissociated state to the breakdown of the hexamer into a pair of dimer and tetramer. While the tetramer form is unstable, it is expected to be more stable than other intermediates such as trimers, which would require the dissociation of the beta sheet that is present in the dimer interface. However, under our experimental conditions, the dimer interface is clearly more thermally stable than the dimer-dimer interface, as verified by our static measurements, since the hexamer population only begins to appear when most of the monomers have already assembled into dimers. In

addition, the tetramer form itself is typically not observed in the native state, likely due to the fact that the most stable dimer-dimer interface form is in the hexamer state.[36,37] This agrees with our observation that the tetramer does not appear as a discrete state in the static SAXS data, which demonstrates presence of only hexamers, dimers and monomers. A more robust verification of the tetramer state is precluded due to the lack of crystal structure data for it.[40]

steps during dissociation occur on significantly shorter timescales than those that occur during dimer dissociation, despite the former occurring at lower temperatures than the latter. In addition, the hexamer dissociation steps are slower than the dimer, and happen stepwise, first through formation of a tetramer and dimer intermediates and then a complete dissociation into dimers. The differences between dimer and hexamer formation processes likely originate from the

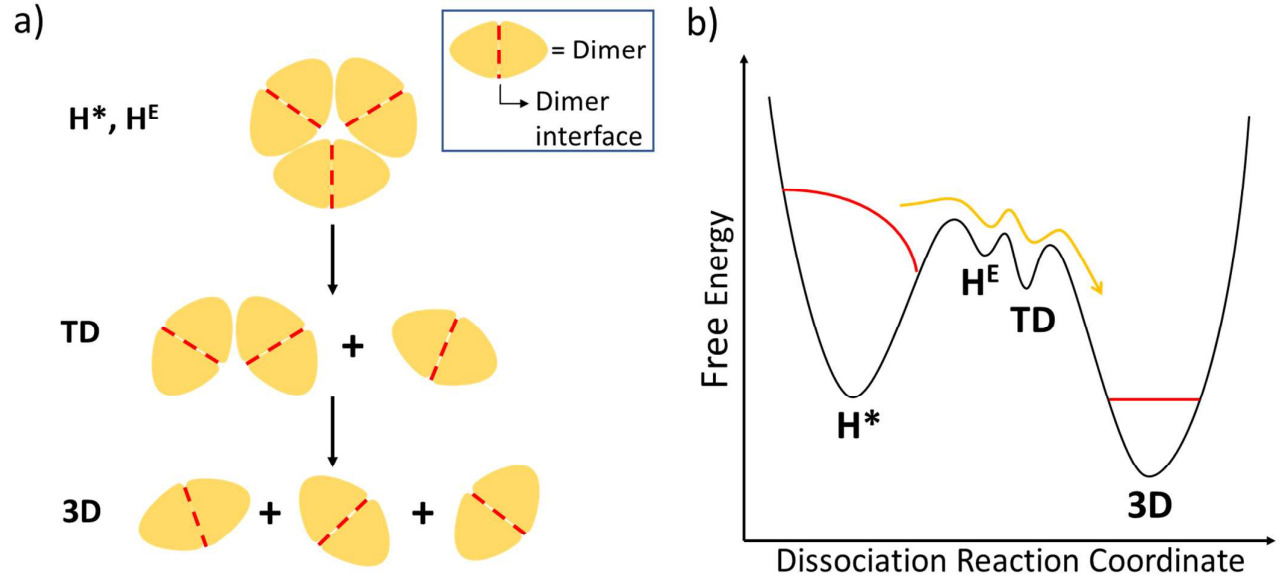

Figure 4. (a) Scheme of the proposed insulin associative states that appear during the oligomer dissociation process following T-jump. (b) Proposed schematic free energy landscape immediately following the T-jump representative of unfolding (dissociation) dynamics. Following the T-jump the insulin population is in a non-equilibrium over-populated hexamer state which proceeds to dissociates through a mechanism involving several high energy intermediates that are transiently populated during the reaction. The red curves indicate the populations in the initial non-equilibrium hexamer and dimer states immediately after the T-jump, the yellow arrow depicts the reaction pathway towards equilibrium.

The proposed dissociation mechanism and schematic free-energy landscape[41–44] of the T-jump induced dissociation reaction are summarised in figure 4. Immediately following the T-jump the hexamer adopts a hot state that is slightly expanded due to loss of hydrogen bonding. Following this state, the hexamer unfolds to become more expanded and flexible while still retaining its constituent dimer subunits. On longer timescales, the hexamer unfolds to form pairs of dimers and tetramers, followed by tetramer dissociation into dimers. As both hexamers and dimers present expanded intermediate states prior to dissociation, it is possible that similar processes occur during tetramer dissociation. However, such processes are likely too fast (i.e. nanoseconds to microseconds) to be captured by our experiment as they are obscured by the millisecond timescale of hexamer dissociation into tetramer-dimer pairs.

A comparison between the structural dynamics of dimer and hexamer dissociation processes reveals appreciable differences between them, in particular in the number of intermediates and timescales involved. Insulin dimer dissociation proceeds through the adoption of multiple intermediates, including two reorganization steps, followed by a single dissociation step.[15] In contrast, hexamer dissociation proceeds through a single reorganization step followed by two dissociation steps. Moreover, the hexamer reorganization different nature of interaction between the constituent units. Dimer formation occurs through the formation of an intermolecular beta sheet, which requires a degree of cooperative refolding of the monomers into the dimer, while the formation of hexamers involves the assembly of dimer-dimer interfaces, typically also around Zn^{2+} ions.

While the states observed in our study (H^E, TD, 3D) are expected to be related to the association mechanism by virtue of microscopic reversibility[14,45–48], these states might only represent a partial picture of the association process. As previously stated, T-jumps are particularly sensitive to the late stages of association, whereas processes such as diffusion and, possibly, induced fit states, which represent early steps in association, may not be captured by our current study.[14] Therefore, our proposed model does not proport to represent the totality of the associative process, but rather more indicative of the later stages in association.

Finally, from investigating these dissociation dynamics we learn that the final stages of insulin association involve the adoption of an extended associated intermediate state, regardless of whether the process involves association of monomers into dimers or dimers into hexamers. These expanded intermediates quickly evolve into the final compact state by internal restructuring and folding process. This final step is likely involved in the prevention of misfolded states,

such as fibrils, which are formed from extended subunits, but not from compact ones.[8] It is possible that destabilization of this final process is contributing to the formation of undesirable fibrils.

Conclusions

From our study of hexamer dissociation dynamics induced by T-jump we have gained insights into the short-lived intermediates that appear at the final stages of the insulin hexamer association process. We found that hexamer association from the dimer state evolves through the adoption of multiple associative states and intermediates within those states. While the appearance of a tetramer state in insulin has been previously concluded, to the best of our knowledge the short-lived expanded intermediate, the H^E state, has not previously been reported. The appearance of this transient state provides insights into the mechanism of quaternary structure evolution, namely that the constituent subunits come together prior to folding into a more stable, less flexible form and that these processes are consecutive rather than parallel and mimic a similar process that has been previously reported for dimers by induced fit mechanism. The finding that a majority of the folding and loss of flexibility occurs after units have already come together implies that cooperative folding requires some preferred interactions, likely at the interfaces between the units and that disruption of this process can lead to undesirable outcomes, such as the formation of fibrils. Moreover, it is apparent that insulin association dynamics deviate from simple two-state kinetics regardless of the mechanism by which the constituent subunits associate. Finally, these findings are evidence for the utility of ultrafast T-jump experiments coupled with a structural probe in the understanding of protein-protein interactions, as well as protein folding mechanisms.

Conflicts of interest

There are no conflicts to declare.

Acknowledgements

This work was supported by the National Institute of Health, under Contract No. R01-GM115761. B.A. acknowledges support from the U.S. Department of Energy (DOE), Office of Science Graduate Student Research program, administered by the Oak Ridge Institute for Science and Education, managed by ORAU under contract number DE-SC0014664, as well as from the U.S. DOE Office of Science, Office of Basic Energy Science, under award number DE-SC0016288. This research used resources of the APS, a U.S. DOE Office of Science User Facility operated for the DOE Office of Science by Argonne National Laboratory under Contract No. DE-AC02-06CH11357. Use of BioCARS was also supported by the National Institute of General Medical Sciences of the National Institutes of Health under grant number R24GM111072. The content is solely the responsibility of the authors and does not necessarily represent the official views of the National Institutes of Health. Time-resolved set-up at Sector 14 was funded in part through a collaboration with Philip Anfinrud (NIH/NIDDK). Optical equipment used for IR beam delivery at BioCARS was purchased with support from the Fraser lab at University of California San Francisco. We would also like to acknowledge Guy Macha (BioCARS) for his assistance in designing the sample holder. Portions of this work were performed at the DuPont-Northwestern-Dow Collaborative Access Team (DND-CAT) located at Sector 5 of the APS. DND-CAT is supported by Northwestern University, E.I. DuPont de Nemours & Co., and The Dow Chemical Company. Data was collected using an instrument funded by the National Science Foundation under Award Number 0960140.

Notes and references

1 I. M. A. Nooren and J. M. Thornton, Structural characterisation and functional significance of transient protein-protein interactions, *J. Mol. Biol.*, 2003, **325**, 991–1018.

2 M. C. Carpenter and D. E. Wilcox, Thermodynamics of Formation of the Insulin Hexamer: Metal-Stabilized Proton-Coupled Assembly of Quaternary Structure, *Biochemistry*, 2014, **53**, 1296–1301.

3 Y. Hong, L. Meng, S. Chen, C. W. T. Leung, L.-T. Da, M. Faisal, D.-A. Silva, J. Liu, J. W. Y. Lam, X. Huang and B. Z. Tang, Monitoring and Inhibition of Insulin Fibrillation by a Small Organic Fluorogen with Aggregation-Induced Emission Characteristics, *J. Am. Chem. Soc.*, 2012, **134**, 1680–1689.

4 J. F. Smith, T. P. J. Knowles, C. M. Dobson, C. E. MacPhee and M. E. Welland, Characterization of the nanoscale properties of individual amyloid fibrils, *Proc. Natl. Acad. Sci.*, 2006, **103**, 15806–15811.

5 G. D. Smith, W. A. Pangborn and R. H. Blessing, The structure of T 6 bovine insulin, *Acta Crystallogr. Sect. D Biol. Crystallogr.*, 2005, **61**, 1476–1482.

6 Y. Xu, Y. Yan, D. Seeman, L. Sun and P. L. Dubin, Multimerization and Aggregation of Native-State Insulin: Effect of Zinc, *Langmuir*, 2012, **28**, 579–586.

7 G. Dodson and D. Steiner, The role of assembly in insulin's biosynthesis., *Curr. Opin. Struct. Biol.*, 1998, **8**, 189–94.

8 A. Ahmad, I. S. Millett, S. Doniach, V. N. Uversky and A. L. Fink, Partially folded intermediates in insulin fibrillation, *Biochemistry*, 2003, **42**, 11404–11416.

9 V. N. Uversky, L. N. Garriques, I. S. Millett, S. Frokjaer, J. Brange, S. Doniach and A. L. Fink, Prediction of the association state of insulin using spectral parameters, *J. Pharm. Sci.*, 2003, **92**, 847–858.

10 L. Nielsen, R. Khurana, A. Coats, S. Frokjaer, J. Brange, S. Vyas, V. N. Uversky and A. L. Fink, Effect of Environmental Factors on the Kinetics of Insulin Fibril Formation: Elucidation of the Molecular Mechanism, *Biochemistry*,

2001, **40**, 6036–6046.

11 Z. Ganim, K. C. Jones and A. Tokmakoff, Insulin dimer dissociation and unfolding revealed by amide I two-dimensional infrared spectroscopy, *Phys. Chem. Chem. Phys.*, 2010, **12**, 3579–3588.

12 W. Bocian, J. Sitkowski, E. Bednarek, A. Tarnowska, R. Kawęcki and L. Kozerski, Structure of human insulin monomer in water/acetonitrile solution, *J. Biomol. NMR*, 2008, **40**, 55–64.

13 A. K. Attri, C. Fernández and A. P. Minton, pH-dependent self-association of zinc-free insulin characterized by concentration-gradient static light scattering, *Biophys. Chem.*, 2010, **148**, 28–33.

14 X.-X. Zhang, K. C. Jones, A. Fitzpatrick, C. S. Peng, C.-J. Feng, C. R. Baiz and A. Tokmakoff, Studying Protein–Protein Binding through T-Jump Induced Dissociation: Transient 2D IR Spectroscopy of Insulin Dimer, *J. Phys. Chem. B*, 2016, **120**, 5134–5145.

15 D. Rimmerman, D. Leshchev, D. J. Hsu, J. Hong, I. Kosheleva and L. X. Chen, Direct Observation of Insulin Association Dynamics with Time-Resolved X-ray Scattering, *J. Phys. Chem. Lett.*, 2017, **8**, 4413–4418.

16 J. Kubelka, Time-resolved methods in biophysics. 9. Laser temperature-jump methods for investigating biomolecular dynamics, *Photochem. Photobiol. Sci.*, 2009, **8**, 499.

17 T. Gensch and C. Viappiani, Time-resolved photothermal methods: accessing time-resolved thermodynamics of photoinduced processes in chemistry and biology, *Photochem. Photobiol. Sci.*, 2003, **2**, 699.

18 J. Pérez and Y. Nishino, Advances in X-ray scattering: From solution SAXS to achievements with coherent beams, *Curr. Opin. Struct. Biol.*, 2012, **22**, 670–678.

19 D. Sato, H. Ohtomo, Y. Yamada, T. Hikima, A. Kurobe, K. Fujiwara and M. Ikeguchi, Ferritin Assembly Revisited: A Time-Resolved Small-Angle X-ray Scattering Study, *Biochemistry*, 2016, **55**, 287–293.

20 S. Akiyama, S. Takahashi, T. Kimura, K. Ishimori, I. Morishima, Y. Nishikawa and T. Fujisawa, Conformational landscape of cytochrome c folding studied by microsecond-resolved small-angle x-ray scattering., *Proc. Natl. Acad. Sci. U. S. A.*, 2002, **99**, 1329–34.

21 H. S. Cho, N. Dashdorj, F. Schotte, T. Graber, R. Henning and P. Anfinrud, Protein structural dynamics in solution unveiled via 100-ps time-resolved x-ray scattering., *Proc. Natl. Acad. Sci. U. S. A.*, 2010, **107**, 7281–6.

22 H. S. Cho, F. Schotte, N. Dashdorj, J. Kyndt, R. Henning and P. A. Anfinrud, Picosecond Photobiology: Watching a Signaling Protein Function in Real Time via Time-Resolved Small- and Wide-Angle X-ray Scattering, *J. Am. Chem. Soc.*, 2016, **138**, 8815–8823.

23 K. Y. Oang, J. G. Kim, C. Yang, T. W. Kim, Y. Kim, K. H. Kim, J. Kim and H. Ihee, Conformational Substates of Myoglobin Intermediate Resolved by Picosecond X-ray Solution Scattering, *J. Phys. Chem. Lett.*, 2014, **5**, 804–808.

24 O. Berntsson, R. P. Diensthuber, M. R. Panman, A. Björling, E. Gustavsson, M. Hoernke, A. J. Hughes, L. Henry, S. Niebling, H. Takala, J. A. Ihalainen, G. Newby, S. Kerruth, J. Heberle, M. Liebi, A. Menzel, R. Henning, I. Kosheleva, A. Möglich and S. Westenhoff, Sequential conformational transitions and α-helical supercoiling regulate a sensor histidine kinase, *Nat. Commun.*, 2017, **8**, 284.

25 O. Berntsson, R. P. Diensthuber, M. R. Panman, A. Björling, A. J. Hughes, L. Henry, S. Niebling, G. Newby, M. Liebi, A. Menzel, R. Henning, I. Kosheleva, A. Möglich and S. Westenhoff, Time-Resolved X-Ray Solution Scattering Reveals the Structural Photoactivation of a Light-Oxygen-Voltage Photoreceptor, *Structure*, 2017, **25**, 933–938.e3.

26 M. Cammarata, M. Levantino, F. Schotte, P. a Anfinrud, F. Ewald, J. Choi, A. Cupane, M. Wulff and H. Ihee, Tracking the structural dynamics of proteins in solution using time-resolved wide-angle X-ray scattering., *Nat. Methods*, 2008, **5**, 881–886.

27 T. W. Kim, J. H. Lee, J. Choi, K. H. Kim, L. J. G. W. van Wilderen, L. Guerin, Y. Kim, Y. O. Jung, C. Yang, J. Kim, M. Wulff, J. J. van Thor and H. Ihee, Protein structural dynamics of photoactive yellow protein in solution revealed by pump-probe X-ray solution scattering., *J. Am. Chem. Soc.*, 2012, **134**, 3145–53.

28 J. Kim, K. H. Kim, J. G. Kim, T. W. Kim, Y. Kim and H. Ihee, Anisotropic Picosecond X-ray Solution Scattering from Photoselectively Aligned Protein Molecules, *J. Phys. Chem. Lett.*, 2011, **2**, 350–356.

29 K. H. Kim, S. Muniyappan, K. Y. Oang, J. G. Kim, S. Nozawa, T. Sato, S. Y. Koshihara, R. Henning, I. Kosheleva, H. Ki, Y. Kim, T. W. Kim, J. Kim, S. I. Adachi and H. Ihee, Direct observation of cooperative protein structural dynamics of homodimeric hemoglobin from 100 ps to 10 ms with pump-probe X-ray solution scattering, *J. Am. Chem. Soc.*, 2012, **134**, 7001–7008.

30 H. Ihee, Visualizing solution-phase reaction dynamics with time-resolved X-ray liquidography, *Acc. Chem. Res.*, 2009, **42**, 356–366.

31 M. Cammarata, M. Lorenc, T. K. Kim, J. H. Lee, Q. Y. Kong, E. Pontecorvo, M. Lo Russo, G. Schiró, A. Cupane, M. Wulff and H. Ihee, Impulsive solvent heating probed by picosecond x-ray diffraction, *J. Chem. Phys.*, 2006, **124**, 124504.

32 A. G. Kikhney and D. I. Svergun, A practical guide to small angle X-ray scattering (SAXS) of flexible and intrinsically disordered proteins, *FEBS Lett.*, 2015, **589**, 2570–2577.

33 E. R. Henry and J. Hofrichter, in *Methods in Enzymology*, Academic Press, 1992, vol. 210, pp. 129–192.

34 M. Schmidt, S. Rajagopal, Z. Ren and K. Moffat, Application of Singular Value Decomposition to the Analysis of Time-Resolved Macromolecular X-Ray Data, *Biophys. J.*, 2003, **84**, 2112–2129.

35 K. Y. Oang, C. Yang, S. Muniyappan, J. Kim and H. Ihee, SVD-aided pseudo principal-component analysis: A new method to speed up and improve determination of the optimum kinetic model from time-resolved data, *Struct. Dyn.*, 2017, **4**, 44013.

36 K. Huus, S. Havelund, H. B. Olsen, M. van de Weert and S. Frokjaer, Thermal Dissociation and Unfolding of Insulin, *Biochemistry*, 2005, **44**, 11171–11177.

37 A. Ahmad, I. S. Millett, S. Doniach, V. N. Uversky and A. L. Fink, Stimulation of Insulin Fibrillation by Urea-induced Intermediates, *J. Biol. Chem.*, 2004, **279**, 14999–15013.

38 C. Manoharan and J. Singh, Insulin Loaded PLGA Microspheres: Effect of Zinc Salts on Encapsulation, Release, and Stability, *J. Pharm. Sci.*, 2009, **98**, 529–542.

39 T. Graber, S. Anderson, H. Brewer, Y. S. Chen, H. S. Cho, N. Dashdorj, R. W. Henning, I. Kosheleva, G. MacHa, M. Meron, R. Pahl, Z. Ren, S. Ruan, F. Schotte, V. Šrajer, P. J. Viccaro, F. Westferro, P. Anfinrud and K. Moffat, BioCARS: A synchrotron resource for time-resolved X-ray science, *J. Synchrotron Radiat.*, 2011, **18**, 658–670.

40 T. S. Choi, J. W. Lee, K. S. Jin and H. I. Kim, Amyloid Fibrillation of Insulin under Water-Limited Conditions, *Biophys. J.*, 2014, **107**, 1939–1949.

41 S. Gianni, N. R. Guydosh, F. Khan, T. D. Caldas, U. Mayor, G. W. N. White, M. L. DeMarco, V. Daggett and A. R. Fersht, Unifying features in protein-folding mechanisms, *Proc. Natl. Acad. Sci.*, 2003, **100**, 13286–13291.

42 D. T. Leeson, F. Gai, H. M. Rodriguez, L. M. Gregoret and R. B. Dyer, Protein folding and unfolding on a complex energy landscape, *Proc. Natl. Acad. Sci.*, 2000, **97**, 2527–2532.

43 M. Gruebele, J. Sabelko, R. Ballew and J. Ervin, Laser Temperature Jump Induced Protein Refolding, *Acc. Chem. Res.*, 1998, **31**, 699–707.

44 H. S. Chung, Z. Ganim, K. C. Jones and A. Tokmakoff, Transient 2D IR spectroscopy of ubiquitin unfolding dynamics., *Proc. Natl. Acad. Sci. U. S. A.*, 2007, **104**, 14237–42.

45 M. Gruebele, The fast protein folding problem, *Annu. Rev. Phys. Chem.*, 1999, **50**, 485–516.

46 A. R. Fersht and V. Daggett, Protein Folding and Unfolding at Atomic Resolution, *Cell*, 2002, **108**, 573–582.

47 M. E. McCully, D. A. C. Beck and V. Daggett, Microscopic Reversibility of Protein Folding in Molecular Dynamics Simulations of the Engrailed Homeodomain, *Biochemistry*, 2008, **47**, 7079–7089.

48 V. S. Pande and D. S. Rokhsar, Molecular dynamics simulations of unfolding and refolding of a beta-hairpin fragment of protein G, *Proc. Natl. Acad. Sci.*, 1999, **96**, 9062–9067.